Applied Physics Letters

RESEARCH ARTICLE | MAY 16 2022

High temperature phase transitions in $NaNbO_3$ epitaxial films grown under tensile lattice strain

S. Bin Anooz ; Y. Wang ; P. Petrik ; M. de Oliveira Guimaraes ; M. Schmidbauer ; J. Schwarzkopf

Appl. Phys. Lett. 120, 202901 (2022)
https://doi.org/10.1063/5.0087959

Applied Physics Letters ARTICLE scitation.org/journal/apl

High temperature phase transitions in $NaNbO_3$ epitaxial films grown under tensile lattice strain

Cite as: Appl. Phys. Lett. **120**, 202901 (2022); doi: 10.1063/5.0087959
Submitted: 11 February 2022 · Accepted: 6 May 2022 ·
Published Online: 16 May 2022

S. Bin Anooz,[1,a] Y. Wang,[1,2] P. Petrik,[3,4] M. de Oliveira Guimaraes,[1] M. Schmidbauer,[1] and J. Schwarzkopf[1]

AFFILIATIONS

[1]Leibniz-Institut für Kristallzüchtung (IKZ), Max-Born-Str. 2, 12489 Berlin, Germany
[2]Electronic Materials Research Laboratory, Key Laboratory of the Ministry of Education & International Center for Dielectric Research, School of Electronic Science and Engineering, The International Joint Laboratory for Micro/Nano Manufacturing and Measurement Technology, Xi'an Jiaotong University, 710049 Xi'an, China
[3]Institute for Technical Physics and Materials Science, Centre for Energy Research, Konkoly Thege Miklós Str. 29-33, 1121 Budapest, Hungary
[4]Faculty of Science and Technology, University of Debrecen, P.O. Box 400, Debrecen 4002, Hungary

[a)]**Author to whom correspondence should be addressed:** saud.binanooz@ikz-berlin.de

ABSTRACT

We have investigated high temperature phase transitions in $NaNbO_3$ thin films epitaxially grown under tensile lattice strain on (110) $DyScO_3$ substrates using metal-organic vapor phase epitaxy. At room temperature, a very regular stripe domain pattern consisting of the monoclinic a_1a_2 ferroelectric phase was observed. Temperature-dependent studies of the refractive index and the optical bandgap as well as *in situ* high-resolution x-ray diffraction measurements prove a ferroelectric–ferroelectric phase transition in the range between 250 and 300 °C. The experimental results strongly suggest that the high-temperature phase exhibits a distorted orthorhombic a_1/a_2 crystal symmetry, with the electric polarization vector lying exclusively in the plane. A second phase transition was observed at about 500 °C, which presumably signifies the transition to the paraelectric phase. Both phase transitions show a pronounced temperature-dependent hysteresis, indicating first-order phase transitions.

$NaNbO_3$ based materials have attracted significant interest due to their promising ferro- and piezoelectric properties[1] and are, thus, considered as possible candidates to replace hazardous lead-based materials in piezo-/ferroelectric technological devices. Temperature dependent phase transitions of bulk $NaNbO_3$ have been frequently studied,[2,3] and a complex sequence has been observed in the temperature range from 640 °C down to −100 °C.[3–5] Above 640 °C, $NaNbO_3$ is paraelectric and cubic, while a tetragonal, four orthorhombic, and finally a rhombohedral phase emerges at 640, 575, 520, 480, 360, and 100 °C during field-free cooling, respectively. This complexity is a consequence of the coupling of Nb shifts and the octahedral tilting of oxygen around Na.[6] At room temperature, $NaNbO_3$ is antiferroelectric with orthorhombic Pbcm symmetry; however, by applying a weak external electric field[7] or stress,[8] it can easily be transformed into a ferroelectric state.

In contrast to bulk $NaNbO_3$, hardly any comparable studies can be found for thin films. Thermal phase transitions have been observed for polycrystalline $NaNbO_3$ films,[9–11] while for epitaxial films, the impact of lattice strains on thermal phase transitions has not yet been studied neither experimentally nor theoretically. On the other hand, for perovskite oxides, strain engineering is an effective tool to tune material properties or even generate properties due the strong coupling between lattice distortions and electronic properties. Lattice strain can be easily imparted to thin films by epitaxial growth and have previously been used to intentionally modify electrical and optical properties as well as to shift the phase transition temperature by hundreds of Kelvin in ferroelectric materials.[12,13]

The investigation of strain effects requires the epitaxial growth of fully strained films with smooth surface and low defect density. However, deposition of high-quality, stoichiometric epitaxial films of $NaNbO_3$ is challenging due to the high volatility of the alkali component. Only a few papers have reported the deposition of $NaNbO_3$ thin films by, e.g., pulsed laser deposition[8,14] and magnetron sputtering.[15,16]

On the other hand, metal-organic vapor phase epitaxy (MOVPE) is a promising deposition technique of high technological relevance. In comparison with physical vapor depositions, epitaxial growth takes place close to thermodynamic equilibrium and at comparatively high oxygen partial pressures of typically 10–20 mbar. This provides nearly perfect thin films with smooth surfaces/interfaces and periodic ferroelectric domain patterns.

Recently, we have reported epitaxial growth of high quality $NaNbO_3$ thin films by MOVPE[14,17–20] and found a sequence of phase transitions when the films are grown on various substrates with varying lattice mismatch.[17,21] In particular, fully compressively strained $NaNbO_3$ thin films grown on the $NdGaO_3$ substrate exhibit an orthorhombic c phase with exclusive vertical electrical polarization, which transforms into the inclined monoclinic M_A phase when the epitaxial strain is partially relaxed. On the other hand, the introduction of tensile strain through epitaxial growth on rare-earth scandates ($ReScO_3$) leads to the formation of the monoclinic a_1a_2-phase with pure in-plane electrical polarization.[14,17] In this study, tensile strained epitaxial $NaNbO_3$ films have been grown on the (110) $DyScO_3$ (DSO) substrate. *In situ* high-resolution x-ray diffraction (HR-XRD) and spectroscopic ellipsometry (SE) reveal a first-order phase transition at high temperatures between 250 and 300 °C, with a pronounced hysteresis observed between the heating and cooling processes. Although more detailed investigations are still needed, our data at this stage indicate that the high-temperature phase exhibits a distorted a_1/a_2 orthorhombic symmetry with pure in-plane polarization.

$NaNbO_3$ films with a nominal thickness of about 40 nm were grown on 0.1° off-oriented (110) $DyScO_3$ substrates (CrysTec GmbH Berlin, Source material purity 4 N) by liquid delivery spin MOVPE. Details of the deposition method are given in Ref. 18; however, in the present study, we use slightly different parameters [flash evaporation temperature of 230 °C for the Na(thd) (99.999%) solution and 190 °C for the $Nb(EtO)_5$ (99.999%) solution, a Na-to-Nb concentration ratio in the source liquids of 4 and an O_2-to-Ar ratio of 0.6]. Figure 1(a) shows an atomic force micrograph (AFM; Bruker Dimension Icon) of such a 40 nm $NaNbO_3$ film. The surface morphology mimics the step structure of the substrate prior to growth due to 0.1° off-orientation, i.e., it is formed of regularly spaced surface steps, indicating a step-flow growth mode with a very low root mean square (rms) surface roughness of about 0.14 nm. A piezoresponse force microscope (PFM) equipped with a dual AC resonance tracking (DART) mode (Asylum Research MFP-3D stand-alone instrument) was applied to image the ferroelectric domains. Lateral PFM measurements presented in Fig. 1(b) reveal a periodic stripe domain pattern where the stripes are aligned along the $[1\bar{1}0]_{DSO}$ direction of the substrate. The bright/yellow and dark/black means that the in-plane polarization vector has a component along the $[1\bar{1}0]_{DSO}$ and $[\bar{1}10]_{DSO}$ directions, respectively.[22] In contrast, the corresponding vertical PFM image (not shown here) exhibits no significant signal, proving that the electric polarization vector is aligned exclusively in the film plane. These results are consistent with the formation of ferroelectric a_1a_2 domains as described in our previous publications.[14,17,20]

At room temperature, the (110) $DyScO_3$ substrate exhibits an orthorhombic symmetry [$a = 5.4424$ Å, $b = 5.7194$ Å, $c = 7.9043$ Å (Ref. 21)] with a nearly quadratic surface unit cell with in-plane lattice parameters of 3.948 and 3.952 Å along the $[1\bar{1}0]_{DSO}$ and $[001]_{DSO}$ directions, respectively. In *Pbcm* symmetry, the orthorhombic lattice parameters of $NaNbO_3$ are given by $a_{NNO} = 5.5047$ Å, $b_{NNO} = 5.5687$ Å, and $c_{NNO} = 15.523$ Å.[23] For reasons of simplicity, we use the pseudocubic (pc) notation[24] with lattice parameters $a_{pc} = 3.881$ Å and $b_{pc} = c_{pc} = 3.915$ Å and $\alpha_{pc} = 89.34°$ being the angle between the b_{pc} and c_{pc} directions [Fig. 1(c)]. The main pseudocubic axes of the epitaxial $NaNbO_3$ film are parallel to the in-plane substrate directions $[1\bar{1}0]_{DSO}$ and $[001]_{DSO}$. For more details, see Ref. 17.

The requirement of elastic energy minimization suggests $(100)_{pc}$ orientation of the pseudocubic unit cell of $NaNbO_3$.[17] Hence, the $NaNbO_3$ film experiences anisotropic tensile lattice strain of 0.81% and 0.94% in $[1\bar{1}0]_{DSO}$ and $[001]_{DSO}$ directions, respectively. We have carried out HR-XRD on a Rigaku 9 kW SmartLab diffractometer using Cu $K_{\alpha 1}$ radiation. In Fig. 2(a), a 2θ–ω scan around the symmetrical out-of-plane $(110)_{DSO}$ Bragg reflection is shown. The $NaNbO_3$ film peak appears at slightly larger 2θ values than the expected bulk values for $(100)_{pc}$ and $(001)_{pc}$ oriented $NaNbO_3$ (marked as blue dashed lines), which proves the presence of tensile in-plane strain. Pronounced thickness fringes are observed, attesting that the film surface and film–substrate interface are smooth. A careful analysis leads to a film thickness of $t = 42.5 \pm 0.5$ nm. Supplementary grazing-incidence in-plane x-ray diffraction in the vicinity of the $[2\bar{2}0]_{DSO}$ Bragg reflection [Fig. 2(b)] shows a clear splitting of the film peaks (P1, P2) as it is characteristic for a $(100)_{pc}$ orientation and a

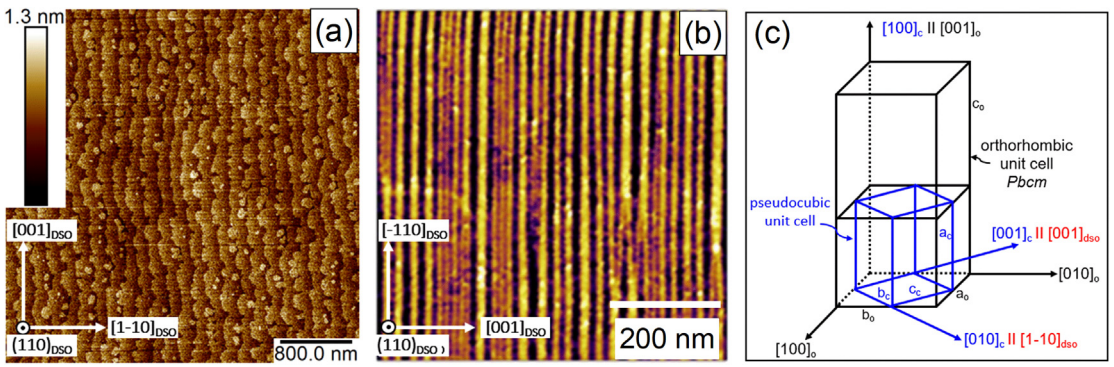

FIG. 1. (a) Atomic force micrograph and (b) lateral piezoresponse force micrograph (phase image) of the $NaNbO_3$ strained film grown on the (110) $DyScO_3$ substrate. (c) Schematic presentation of the orthorhombic (black lines) and inscribed pseudocubic unit cell (blue lines) of $NaNbO_3$ for Pbcm symmetry.

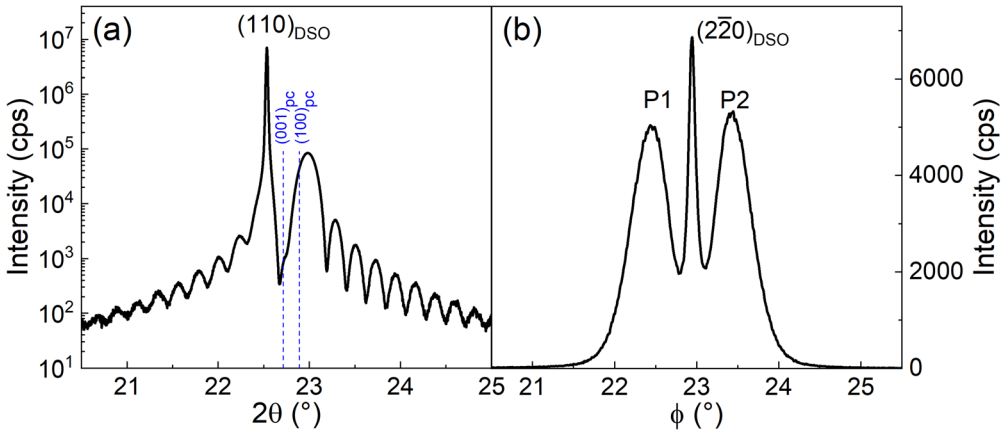

FIG. 2. (a) 2θ–ω scan around the symmetrical $(110)_{DSO}$ out-of-plane Bragg reflection. (b) Grazing incidence x-ray diffraction (angular ϕ-scan) in the vicinity of the $(2\bar{2}0)_{DSO}$ in-plane Bragg reflection.

monoclinic in-plane shearing of the pseudocubic unit cells axes, which is referred to as a_1a_2 phase.[14,17–20] From the angular splitting, we were able to determine the in-plane monoclinic angle to be $\alpha = 89.50° \pm 0.1°$, which fits to the results obtained in Ref. 14 (see Fig. 4 therein). From the peak width, a mean domain width along $[001]_{DSO}$ of about $w = 18(1)$ nm can be evaluated in agreement with the PFM measurements in Fig. 1(b).

The optical properties of the $NaNbO_3$ thin film were determined by SE using a Woollam M-2000DI rotating compensator ellipsometer in the spectral range of 0.73–6 eV at various angles of incidence 60°, 65°, and 70°. To identify the phase transition in the epitaxial $NaNbO_3$ film, temperature dependent SE measurements were performed from room temperature up to 560 °C. To evaluate the refractive index and bandgap energy, we used a model to fit the SE parameters, ψ and Δ, which consists of a four-component stack composed of substrate/film/surface roughness/air. The optical properties of the surface roughness layer are analyzed by a Bruggeman effective medium approximation[25] consisting of a 50% bulk film/50% void mixture. An analytical model using the Tauc–Lorentz (TL) dispersion relations[26] model was employed to determine the dielectric function and layer thicknesses (see the supplementary material). The TL parameterization is more realistic for the optical functions of amorphous materials.[26] However, it has been successfully applied to crystalline material.[27,28] To meet our main objective of detecting the phase transition from temperature dependent SE measurements, we found that the use of TL dispersion is adequate to fit the ellipsometric data of the $NaNbO_3$ film. The obtained film thickness of $t = (43.5 \pm 0.4)$ nm is in good agreement with the x-ray data ($t = 42.5 \pm 0.5$ nm), and a surface roughness of about (0.40 ± 0.04) nm could be determined. Room temperature SE measurements performed at several angles of incidence of 60°, 65°, and 70° and sample orientations (supplementary material, Fig. S1) revealed only a weak dependence of the refractive index (n) and the extinction coefficient (k) (supplementary material, Fig. S2), further details are provided in supplementary. Therefore, in the following, we focus on results obtained at an angle of incidence of 70°, and an isotropic model was throughout used for all temperature-dependent SE measurements.

Figures 3(a) and 3(b) show the temperature dependence of the real (ε_r) and imaginary (ε_i) parts of the dielectric function, respectively,

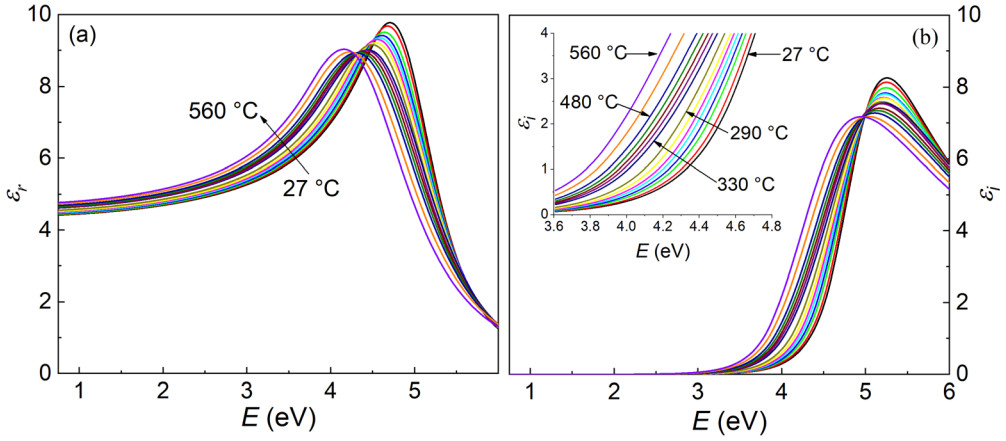

FIG. 3. (a) Real (ε_r) and (b) imaginary (ε_i) parts of the dielectric function as a function of photon energy in the epitaxial $NaNbO_3$ film on the $DyScO_3$ substrate on heating from 27 °C up to 560 °C.

of the $NaNbO_3$ film as a function of the photon energy. For $NaNbO_3$, the valence band is primarily constituted by the O 2p states, while the conduction band derives from the transition-metal (Nb) *d* orbitals. The *d* band consists of a lower energy, wide $d\varepsilon$ sub-band and a higher energy, narrower $d\gamma$ sub-band. The dielectric maximum (imaginary part at 27 °C) at about 5.5 eV is dominated by the valence band → $d\varepsilon$ transition.[29] To clarify the shift of the absorption edge around the phase transitions, the imaginary part ε_i at the absorption edge has been recorded as function of the temperature, as marked [inset of Fig. 3(b)]. The experimental spectra agree with those typically observed in the transparency range of perovskite oxide ferroelectrics and comparable to that of the $NaNbO_3$ film deposited on $DyScO_3$.[19,29] In the near-infrared range, the real part slightly increases with temperature, while at the UV-visible region, the imaginary part shows a redshift tendency. This behavior is attributed to electron–phonon interaction that is enhanced with the increasing temperature, as observed in other ferroelectric materials.[30]

The evaluated *n* at 3.2 eV and the bandgap energy (E_g) of $NaNbO_3$ as a function of temperature on heating and cooling are presented in Figs. 4(a) and 4(b), respectively. The refractive index is graphed at an energy of 3.2 eV, i.e., near the bandgap 3.9 eV, to best observe variations with phase transitions and structural changes.[9,31] The refractive index at 3.2 eV of a bare $DyScO_3$ substrate is additionally shown in Fig. 4(a) as a reference. It reveals a linear dependency as expected for a dielectric material without phase transition. In contrast, the spectra of $NaNbO_3$ show significant deviations from linearity near 305 and 520 °C on heating, indicating the occurrence of phase transitions. Furthermore, during the cooling cycle (blue dotted curves), the deviations from linear behavior occur at lower temperatures, resulting in a pronounced hysteresis loop with a width of about 50 K around the phase transitions at 305 and 520 °C (Fig. 4).

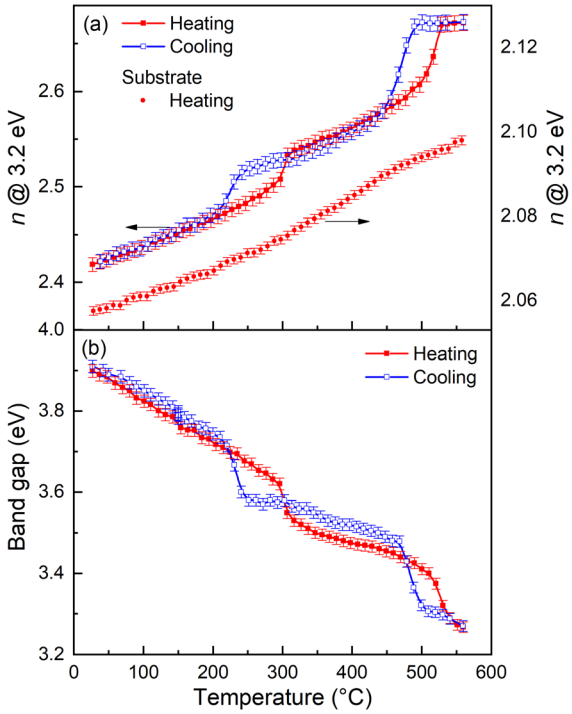

FIG. 4. (a) Refractive index of $NaNbO_3$ as a function of temperature on heating and cooling and of the $DyScO_3$ substrate on heating, (b) optical bandgap of $NaNbO_3$ as a function of temperature on heating and cooling.

The bandgap energy of $NaNbO_3$ film was estimated from the onset of the main electronic absorption (TL) as well as from the Tauc-plot along the $[001]_{DSO}$ and $[1\bar{1}0]_{DSO}$ directions (see the supplementary material for further discussion). Density functional theory calculations of the electronic properties of orthorhombic $NaNbO_3$ revealed that $NaNbO_3$ has an indirect bandgap.[32] Therefore, we will discuss the estimated indirect bandgap of the $NaNbO_3$ film with the reported indirect bandgaps. From Table S2 of the supplementary material, it is clear that the average of the estimated indirect bandgap (Tauc-plot) along the [001] and $[1\bar{1}0]$ directions is (4.04 ± 0.02) eV. This value is larger than the indirect bandgap of 3.45[32] eV (Tauc-plot) and 3.39 eV and 3.86[33] eV estimated using the double TL-dispersion of $NaNbO_3$. Eng *et al.*[34] reported that the increase in the Nb–O–Nb bond angle by applying tensile strain leads to an increase in the conduction bandwidth, and hence, the bandgap decreases. However, this has not been observed for our $NaNbO_3$ thin films, where the bandgap increases under tensile strain. This increase is tentatively explained by the ferroelectric polarization induced by the tensile lattice strain, which leads to an additional bandgap widening.[35,36] On the other hand, the decrease in the bandgap with increasing temperature is related to the temperature-dependent dilatation of the lattice, whereas the majority contribution comes from the electron lattice interaction.[37] With the increase in temperature between room temperature and about 320 °C, and further from 320 to 500 °C, the decrease in the optical bandgap can be fitted by a linear approximation with $\delta E_g/\delta T = -1$ meV/K and $\delta E_g/\delta T = -0.6$ meV/K, respectively, these values are in good agreement with values of other ferroelectric perovskites.[38] The slight difference between these values additionally indicates the existence of two different phases in this temperature range.

To elucidate the structural changes associated with the observed phase transitions, *in situ* x-ray reciprocal space mappings (RSMs) were recorded from room temperature up to 550 °C. We have chosen the asymmetric $(444)_{DSO}$ substrate Bragg reflection, which is sensitive to both vertical and horizontal normal strain components as well as to shear strains. In this scattering geometry, the in-plane component Q_x of the scattering vector is parallel to the $[001]_{DSO}$ direction of the $DyScO_3$ substrate while the out-of-plane component Q_z is oriented along the surface normal of the $(110)_{DSO}$ plane. Selected RSMs presented in Figs. 5(a)–5(f) reveal the following sequence:

(i) From room temperature up to 300 °C, a single film Bragg reflection is observed, which occurs at larger vertical scattering component Q_z but identical horizontal scattering component Q_x as the $(444)_{DSO}$ substrate Bragg reflection. Together with the results from Fig. 1, this is in accordance with the presence of an a_1a_2 phase in the films and proves that the film is fully tensile strained on the $DyScO_3$ substrate.

(ii) Increasing the temperature to 320 °C, the film peak exhibits a pronounced horizontal splitting. This is attributed to a change in the thin film crystal symmetry and indicates a structural phase transition between 300 and 320 °C, which is in good agreement with the SE measurements (Fig. 4). The center of mass of the doubled film peaks is slightly

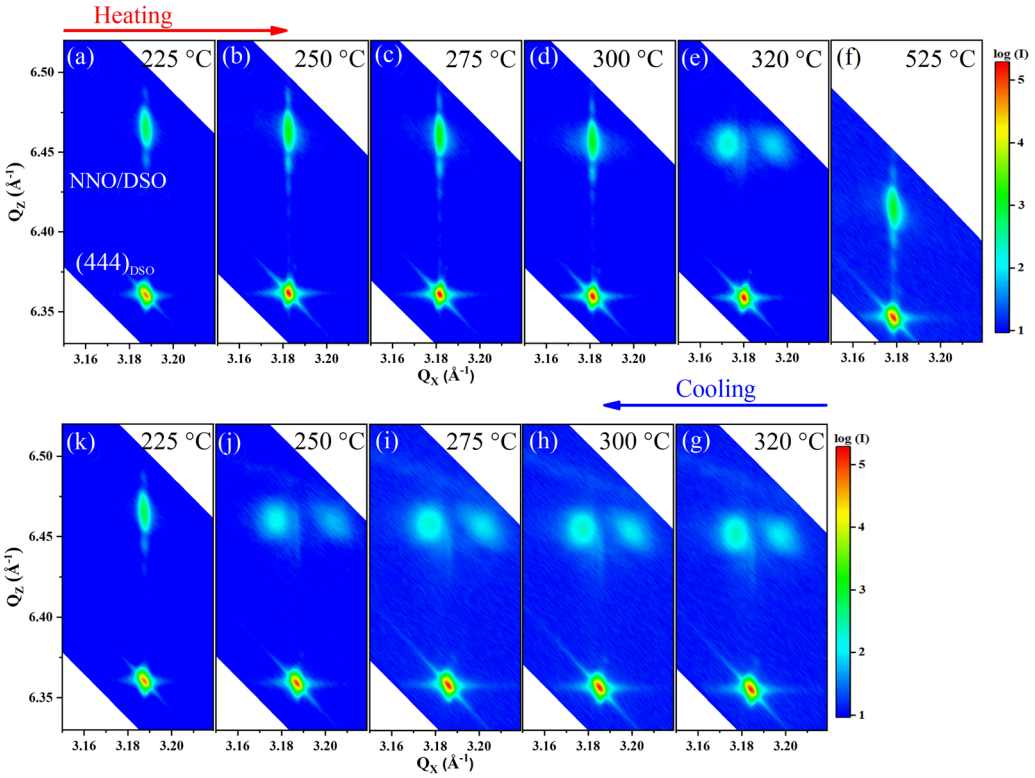

FIG. 5. X-ray reciprocal space maps of the $NaNbO_3$ film in the vicinity of the asymmetrical $(444)_{DSO}$ Bragg reflection of the $DyScO_3$ substrate (a)–(f) on heating, and, (g)–(k) on cooling.

shifted toward larger Q_x values as compared to the substrate peak, indicating a slightly reduced horizontal lattice spacing.

(iii) The horizontal splitting persists up to 500 °C, while above 500 °C it disappears, leaving a single film peak that appears at identical Q_x value as the substrate peak. This is a fingerprint of a second structural phase transition at about 500 °C, which fits well to the SE measurements described above in Fig. 4.

(iv) During the cooling cycle [Figs. 5(g)–5(k)], the phase transition occurs at lower temperatures. This hysteretic behavior implies a first order phase transition and corresponds well to the behavior of n(T) and E_g(T) in Fig. 4.

The horizontal peak splitting displayed in Figs. 5(e) and 5(g)–5(j) indicates the presence of a distorted orthorhombic in-plane a_1/a_2 ferroelectric phase, similar to the one observed in strained $K_{0.9}Na_{0.1}NbO_3$ thin films grown on the (110) $NdScO_3$ substrate.[39,40] Indeed, neglecting the octahedral tilting in $NaNbO_3$ (as opposed to $K_xNa_{1-x}NbO_3$ with $x \geq 0.5$), one would expect a similar phase transition path for the $NaNbO_3$ thin film grown on $DyScO_3$. A further indication of an exclusively in-plane ferroelectric-to-ferroelectric phase transition ($a_1a_2 \rightarrow a_1/a_2$) can be seen in the behavior of the out-of-plane lattice parameter, which shows no detectable signature across the phase transition. In contrast, such a signature can be detected, for example, in compressively strained $K_{0.7}Na_{0.3}NbO_3$ thin films on $TbScO_3$, which exhibits a strong vertical polarization component both at room temperature (M_C-phase) and at high temperatures (c-phase).[13] The second phase transition observed at about 500 °C is presumably a transition to the paraelectric phase, which again show a pronounced hysteretic behavior. In any case, further detailed investigations are required for a more accurate characterization of the high-temperature phases.

To conclude, we have investigated tensile strained $NaNbO_3$ thin films grown by MOVPE on the (110) $DyScO_3$ substrate. At room temperature, we observe a very regular stripe domain pattern consisting of the monoclinic a_1a_2 ferroelectric phase with exclusive in-plane electrical polarization. Temperature-dependent refractive index and optical bandgap measurements as well as *in situ* HR-XRD measurements show a ferroelectric-to-ferroelectric phase transition between 250 and 300 °C. Our experimental data strongly suggest that the high temperature phase exhibits a distorted orthorhombic a_1/a_2 symmetry with pure in-plane polarization presumably along $[1\bar{1}0]_{DSO}$ and $[001]_{DSO}$. In addition, a subsequent phase transition presumably to the paraelectric phase was observed at about 500 °C. For both transitions, a pronounced hysteretic behavior was observed, suggesting first-order phase transitions. Our observations on strained films differ significantly from the behavior of $NaNbO_3$ bulk crystals, where a much more complicated scenario takes place.[2,3,5,6] Unfortunately, due to the high complexity of the $NaNbO_3$ crystal structure, no corresponding theoretical studies are available so far. For room temperature, only first-principles studies of possible stable ferroelectric phases as a function of strain are available.[41] Recently, these studies have been

extended to include anisotropic strain and the tilt of oxygen octahedra.[42] However, there are no calculations of temperature–strain phase diagrams or 3D phase field simulations, which have already been carried out very successfully for the simpler $K_xNa_{1-x}NbO_3$ ($x \geq 0.5$) material system.[40,43] Our experimental data tentatively show a similar behavior for strained $NaNbO_3$ and $K_xNa_{1-x}NbO_3$, suggesting that in epitaxial thin films, lattice strain has a larger impact on domain formation than octahedral tiltings. A comparison of our experimental data with such 3D phase field simulations would be highly interesting in view of the apparent similarities of the observed phases and phase transitions in strained $NaNbO_3$ and $K_xNa_{1-x}NbO_3$ thin films.

See the supplementary material for the SE measurements at various angles of incidence, sample rotations and using the interface layer on the model.

We thank the European Regional Development Fund (ERDF) (Project No. 1.8/15) for funding this project. The $DyScO_3$ substrates have been grown at the Leibniz-Institut für Kristallzüchtung in the group of S. Ganschow. P. Petrik is grateful for the support from the Hungarian National Science Fund (OTKA Grant No. K131515). The authors express their gratitude to Dr. S. Ganschow from the Leibniz-Institut für Kristallzüchtung for critical reading of the manuscript.

AUTHOR DECLARATIONS

Conflict of Interest

The authors have no conflicts to disclose.

DATA AVAILABILITY

The data that support the findings of this study are available from the corresponding author upon reasonable request.

REFERENCES

[1]Y. Saito, H. Takao, T. Tani, T. Nonoyama, K. Takatori, T. Homma, T. Nagaya, and M. Nakamura, Nature **432**, 84 (2004).
[2]H. Guo, H. Shimizu, and C. A. Randall, Appl. Phys. Lett. **107**, 112904 (2015).
[3]G. Shirane, R. Newnham, and R. Pepinsky, Phys. Rev. **96**, 581 (1954).
[4]E. A. Wood, Acta Cryst. **4**, 353 (1951).
[5]H. D. Megaw, Ferroelectrics **7**, 87 (1974).
[6]C. N. W. Darlington and H. D. Megaw, Acta Crystallogr., Sect. B **29**, 2171 (1973).
[7]A. Kohori, S. Yamazoe, T. Imai, H. Adachi, and T. Wada, Appl. Phys. Lett. **102**, 112909 (2013).
[8]S. Yamazoe, A. Kohori, H. Sakurai, Y. Kitanaka, Y. Noguchi, M. Miyayama, and T. Wada, J. Appl. Phys. **112**, 052007 (2012).
[9]I. Aulika, A. Dejneka, A. Lynnyk, V. Zauls, and M. Kundzins, Phys. Status Solidi C **6**, 2765 (2009).
[10]I. Aulika, A. Deyneka, V. Zauls, and K. Kundzins, J. Phys: Conf. Ser. **93**, 012016 (2007).
[11]A. V. Pavlenko, D. V. Stryukov, M. V. Vladimirov, A. E. Ganzha, S. A. Udovenko, A. Joseph, J. Sunil, C. Narayana, R. G. Burkovsky, I. P. Raevski, and N. V. Ter-Oganessian, arXiv:2112.04579 (2021).
[12]R. Xu, J. Huang, E. S. Barnard, S. S. Hong, P. Singh, E. K. Wong, T. Jansen, V. Harbola, J. Xiao, B. Y. Wang, S. Crossley, D. Lu, S. Liu, and H. Y. Hwang, Nat. Commun. **11**, 3141 (2020).
[13]L. von Helden, L. Bogula, P. E. Janolin, M. Hanke, T. Breuer, M. Schmidbauer, S. Ganschow, and J. Schwarzkopf, Appl. Phys. Lett. **114**, 232905 (2019).
[14]M. Schmidbauer, J. Sellmann, D. Braun, A. Kwasniewski, A. Duk, and J. Schwarzkopf, Phys. Status Solidi RRL **8**, 522 (2014).
[15]T. Mino, S. Kuwajima, T. Suzuki, I. Kanno, H. Kotera, and K. Wasa, Jpn. J. Appl. Phys., Part 1 **46**, 6960 (2007).
[16]V. Lingwal and N. S. Panwar, J. Appl. Phys. **94**, 4571 (2003).
[17]J. Schwarzkopf, D. Braun, M. Schmidbauer, A. Duk, and R. Wördenweber, J. Appl. Phys. **115**, 204105 (2014).
[18]J. Schwarzkopf, M. Schmidbauer, T. Remmele, A. Duk, A. Kwasniewski, S. Bin Anooz, A. Devi, and R. Fornari, J. Appl. Crystallogr. **45**, 1015 (2012).
[19]S. Bin Anooz, P. Petrik, M. Schmidbauer, T. Remmele, and J. Schwarzkopf, J. Phys. D: Appl. Phys. **48**, 385303 (2015).
[20]A. Duk, M. Schmidbauer, and J. Schwarzkopf, Appl. Phys. Lett. **102**, 091903 (2013).
[21]M. Schmidbauer, A. Kwasniewski, and J. Schwarzkopf, Acta Crystallogr., Sect. B **68**, 8 (2012).
[22]J. Schwarzkopf, D. Braun, M. Hanke, R. Uecker, and M. Schmidbauer, Front. Mater. **4**, 26 (2017).
[23]M. C. Morris, H. F. McMurdie, E. H. Evans, B. Paretzkin, H. S. Parker, and N. C. Panagiotopoulos, *Standard X-Ray Diffraction Powder Pattern, NBS Monograph 25, Section 18, Data for 58 Substances* (National Bureau of Standards, Gaithersburg, 1981), pp. 64–65.
[24]A. Vailionis, H. Boschker, W. Siemons, E. P. Houwman, D. H. A. Blank, G. Rijnders, and G. Koster, Phys. Rev. B **83**, 064101 (2011).
[25]D. Bruggeman, Ann. Phys. **416**, 636 (1935).
[26]G. E. Jellison and F. A. Modine, Appl. Phys. Lett. **69**, 371 (1996).
[27]Y. J. Cho, N. V. Nguyen, C. A. Richter, J. R. Ehrstein, B. H. Lee, and J. C. Lee, Appl. Phys. Lett. **80**, 1249 (2002).
[28]P. Petrik, Physica B **453**, 2–7 (2014).
[29]M. Tyunina, D. Chvostova, L. D. Yao, A. Dejneka, T. Kocourek, M. Jelinek, and S. van Dijken, Phys. Rev. B **92**, 104101 (2015).
[30]M. Rössle, C. N. Wang, P. Marsik, M. Yazdi-Rizi, K. W. Kim, A. Dubroka, I. Marozau, C. W. Schneider, J. Humlíček, D. Baeriswyl, and C. Bernhard, Phys. Rev. B **88**, 104110 (2013).
[31]Y.-f. Tsay, B. Bendow, and S. S. Mitra, Phys. Rev. B **8**, 2688 (1973).
[32]P. Li, S. Ouyang, G. Xi, T. Kako, and J. Ye, J. Phys. Chem. C **116**, 7621 (2012).
[33]I. Aulika, A. Dejneka, V. Zauls, and K. Kundzinsa, J. Electrochem. Soc. **155**, G209 (2008).
[34]H. W. Eng, P. W. Barnes, B. M. Auer, and P. M. Woodward, J. Solid State Chem. **175**, 94 (2003).
[35]M. DrDomenico and S. H. Wemple, J. Appl. Phys. **40**, 720 (1969).
[36]A. Lynnyk, D. Chvostova, O. Pacherova, T. Kocourek, M. Jelinek, A. Dejneka, and M. Tyunina, Appl. Phys. Lett. **103**, 132901 (2013).
[37]Y. P. Varshni, Physica **34**, 149 (1967).
[38]V. Mishra, A. Sagdeo, V. Kumar, M. K. Warshi, H. M. Rai, S. K. Saxena, D. R. Roy, V. Mishra, R. Kumar, and P. R. Sagdeo, J. Appl. Phys. **122**, 065105 (2017).
[39]L. Bogula, L. von Helden, C. Richter, M. Hanke, J. Schwarzkopf, and M. Schmidbauer, Nano Futures **4**, 035005 (2020).
[40]M. Schmidbauer, L. Bogula, B. Wang, M. Hanke, L. von Helden, A. Ladera, J.-J. Wang, L.-Q. Chen, and J. Schwarzkopf, J. Appl. Phys. **128**, 184101 (2020).
[41]O. Diéguez, K. M. Rabe, and D. Vanderbilt, Phys. Rev. B **72**, 144101 (2005).
[42]K. Patel, S. Prosandeev, B. Xu, C. Xu, and L. Bellaiche, Phys. Rev. B **103**, 094103 (2021).
[43]M.-J. Zhou, B. Wang, A. Ladera, L. Bogula, H.-X. Liu, L.-Q. Chen, and C.-W. Nan, Acta Mater. **215**, 117038 (2021).